Research article

ZnO-NPs/AC composite antibacterial agents with N-halamine glycinate functionalized silica-mesoporous silica coating for water disinfection

Issa M. El Nahhal [a,*], Hayfa H Almutairi [b], Jamil K Salim [a], Fawzi S Kodeh [a], Rana H Idais [a]

[a] Department of Chemistry, Al-Azhar University-Gaza, P O Box 1277, Gaza, Palestine
[b] Department of Chemistry, College of Science. King Faisal University, AlAhsa, PO Box 380, Hofuf, 31982, Saudi Arabia

A B S T R A C T

This work deals with the synthesis, structural characterization and applications of *N*-halamine glycinate functionalized silica-mesoporous silica coated ZnO-NPs/AC composite for water disinfection. Several nanocomposite materials were obtained: ZnO-NPs/AC, ZnO-NPs/AC@SiO$_2$, ZnO-NPs/AC@SiO$_2$@mSiO$_2$, ZnO-NPs@SiO$_2$@mSiO$_2$-Gly and ZnO-NPs@SiO$_2$@mSiO$_2$-*N*-halamine-Gly. These nanocomposite materials were fully characterized via different physiochemical techniques including: FTIR, TGA, XPS, XRD, SEM, TEM and BET. XRD indicated a predominance of crystalline pattern of ZnO-NPs impregnated into activated carbon (AC) and their silica and *m*-mesoporous silica coating precursors. The FTIR spectra confirmed an immense combination between ZnO-NPs and AC of ZnO-NPs/AC nanocomposite as well as its interactions with coated silica precursors. SEM, TEM images illustrated that the fabricated ZnO-NPs/AC nanocomposites are well coated with silica-mesoporous silica functionalized *N*-halamine. The distinctive surface area has decreased from 800 m^2/g for pristine AC to 772 m^2/g for ZnO-NPs/AC and to 282 m^2/g for ZnO-NPs/AC@SiO$_2$ and to 139 m^2/g for ZnO-NPs/AC@SiO$_2$@mSiO$_2$ and to 15.4 m^2/g for ZnO-NPs@SiO$_2$@mSiO$_2$-*N*-Gly. All those nanocomposites showed good efficacy against all four bacterial species, with higher inhibition zones for the 2 g-positive bacteria than that of the 2 g-negative ones. The ZnO@SiO$_2$@mSiO$_2$-*N*-halamine-Gly exhibited the high zone inhibition against all tested bacteria except for *E. Coli*.

1. Introduction

In recent times, the issue of bacteria resistance to most antimicrobial activities has grown significantly. Recently, ZnO nanoparticles have been proposed as a safe and effective material to impart antibacterial activity [1]. New ecologically acceptable methods of producing ZnO-NPs were therefore needed [2–4]. ZnO-NPs' high specific surface area which is enabled by their higher surface reactivity and reduced particle size has been demonstrated to have strong antibacterial potential for a range of microbiological applications [5–7].

The presence of –OH groups on the activated surfaces has enhanced the incorporation of ZnO-NPs with both substrates like

---

* Corresponding author.
E-mail address: i.nahhal@alazhar.edu (I.M. El Nahhal).
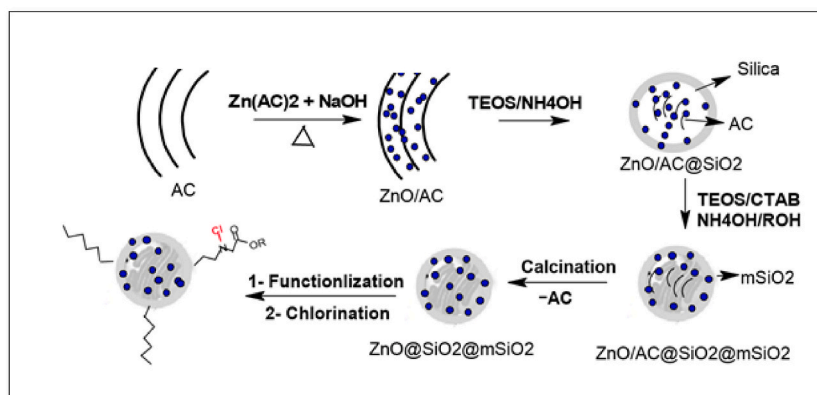
Fig. 1. Schematic preparation description of silica-, mesoporous silica and their *N*-halamine glycinate functionalized coated ZnO-NPs/AC nanocomposite.

activated carbon [8,9] or silica surfaces [10,11]. Due to amazing characteristics of AC that has recently increased such as its significant adsorption capacity, chemical stability and mechanical strength. Therefore, the AC has been used for removal of water pollutants due to its high specific surface area and its interior microporous structure. It has been positioned to be a superb organic contaminant nano- and microscale adsorbent [12]. The presence of adsorbed organic matters within the AC has enhanced the growth of microorganisms inside the activated carbon substrate and increased the microorganism contamination. This has limited its utility for water purification [13,14]. Activated carbon substrate, however, has also demonstrated antibacterial activities when it impregnated with nanometals or nanometal oxides [15–18]. The use of ZnO-NPs is due to it is inert, cheap, non-toxic and biocompatible. In this manner, there has been expanded intrigued in creating green and cost-effective union approaches for ZnO-NPs. ZnO-NPs as safe nanomaterials have been utilized for poison photodegradation and disinfection of microorganism [19]. Later ZnO-NPs altered enacted carbon have been utilized for water sanitization [8,20,21]. The antimicrobial properties of ZnO-NPs can be enhanced when it combined with AC substrate. This is primarily credited to the likely synergistic impact when it combined to AC. In our present research, we have used silica and m-silica for coating the ZnO-NPs/AC nanocomposite for the first time to improve the dispersibility of ZnO-NPs during the fabrication of ZnO/AC@SiO$_2$@mSiO$_2$ composite material. Even though at low level of zinc concentration of ZnO-NPs (20 %) content, these materials achieved a high reduction and very effective towards variety of microorganisms. The use of silica and CTAB was used to improve mechanical, dispersibility and thermal properties.

In this research, the activated carbon modified ZnO-NPs nanocomposite (ZnO-NPs/AC) was first prepared by impregnated ZnO-NPs into activated carbon [21]. Four new nanocomposite materials ZnO-NPs/AC@SiO$_2$, ZnO-NPs/AC@SiO$_2$@mSiO$_2$, ZnO-NPs@-SiO$_2$@mSiO$_2$-Gly and its corresponding *N*-halamine glycinate mesoporous silica ZnO-NPs@SiO$_2$@mSiO$_2$-*N*-halamine-Gly nano-composite material were prepared. The parent ZnO/AC nanocomposite was firstly coated with dense silica layer (ZnO-NPs/AC@SiO$_2$) using Stöber method, followed by coating with mesoporous layer (ZnO-NPs/AC@SiO$_2$@mSiO$_2$). The free AC coated material ZnO-NPs@SiO$_2$@mSiO$_2$ was obtained by etching the AC through calcination of ZnO-NPs/AC@SiO$_2$@mSiO$_2$. The ZnO-NPs@-SiO$_2$@mSiO$_2$-Gly was prepared by functionalization of ZnO-NPs@SiO$_2$@mSiO$_2$ with glycinate silane agent, The ZnO-NPs@-SiO$_2$@mSiO$_2$-*N*-halamine-Gly was obtained by chlorination with sodium hypochlorite solution. Our aim of this work is the preparation of process of ZnO-NPs@SiO$_2$@mSiO$_2$-N-halamine-Gly through the following four steps including: (i) impregnating of ZnO-NPs (ii) silica coating (SiO$_2$) via Stöber method, (iii) mesoporous silica coating (mSiO$_2$) and (iv) functionalization with glycinate silane agent followed by chlorination with sodium hypochlorite solution (Fig. 1). The schematic description of preparation of different nano-composite materials is given in Fig. 1.

2. Materials and methods

2.1. Materials

The following starting chemicals were obtained from Merck without further purification, ethylchloroaectate (ClCH$_2$COOEt), 99 %, tetraethyl orthosilicate (Si(OEt)$_4$, 99 %, 3-aminopropyltrimethoxysilane ((MeO)$_3$Si(CH$_2$)$_3$–NH$_2$), 97 %, potassium iodide (KI), 99.5 %, sodium thiosulfate pentahydrate (Na$_2$S$_2$O$_3$)5H$_2$O, 99 %, and zinc acetate dihydrate (Zn(CH$_3$COO)$_2$)2H$_2$O, 97.5 %. Dehydrated nutrient agar powder and nutrient broth powder were purchased from Difco.

2.2. Preparation of 3-glycinatepropyltrimethoxysilane (Gly-S)

The functionalized 3-glycinatepropyltrimethoxysilane (Gly-S) was prepared as previously reported [22]. The prepared function-alized 3-ethylglycinepropyltrimethoxysilane (Gly-S) material was identified by FTIR spectra.

2.3. Preparation of ZnO-NPs/AC nanocomposite

The ZnO-NPs/AC nanocomposite was prepared as previously reported [23]. The ZnO-NPs/AC nanocomposite was dried in vacuum oven at 100 °C for 24 h (Fig. 1). In this preparation and due to the use NaOH in presence of $NaBH_4$, the Zn $(CH_3COO)_2.H_2O$ precursor is converted into ZnO-NPs/AC at mild temperature of 80 °C to avoid degradation of AC. The chemical structure of ZnO-NPs/AC nanocomposite was clearly identified using FTIR, TGA and XPS methods.

2.4. Preparation of ZnO-NPs/AC@SiO₂ nanocomposite

The ZnO-NPs/AC@SiO_2 nanocomposite was prepared through sol–gel process as previously reported [9,10]. The ZnO-N-Ps/AC@SiO_2 nanocomposite was filtered off, washed with deionized water and ethanol. The chemical structure of silica-coated ZnO-NPs/AC@SiO_2 nanocomposite was clearly identified using FTIR, TGA and XPS methods.

2.5. Preparation of ZnO-NPs/AC@SiO₂@mSiO₂ nanocomposite

The mesoporous coated nanocomposite (ZnO-NPs/AC@SiO_2@$mSiO_2$) was prepared in a similar reported method [9,10] by sol-gel process in presence of TEOS and CTAB as cationic surfactant in an ethanolic solution in presence of ammonia solution. The ZnO-N-Ps/AC@SiO_2@$mSiO_2$ product was filtered off, washed with water and ethanol, then dried at 100 °C for 12 h. The ZnO-NPs@-SiO_2@$mSiO_2$ product was obtained through calcination of ZnO-NPs/AC@SiO_2@$mSiO_2$ at 600 °C for 4 h to remove AC (Fig. 1). The chemical structure of silica-coated ZnO-NPs/AC@SiO_2 nanocomposite was clearly identified using FTIR, TGA and XPS methods.

2.6. Preparation of ZnO-NPs@SiO₂@mSiO₂-Gly. Nanocomposites

The glycinate functionalized ZnO-NPs@SiO_2@$mSiO_2$-Gly nanocomposite material was synthesized in a similar method as previously reported [9,10] by refluxing 0.10 g of ZnO@SiO_2@$mSiO_2$ with 3.5 mL of glycinate silane agent (Gly-S) in 20 mL ethanol for 48 h at 70 °C. The ZnO@SiO_2@$mSiO_2$-Gly composite material was isolated via centrifugation, washed with ethanol and dried in a vacuum at 80 °C for 4 h (Fig. 1). The corresponding N-halamine-glycinate functionalized nanocomposite ZnO-NPs@SiO_2@$mSiO_2$-Cl-Gly was formed by chlorination of ZnO-NPs@SiO_2@$mSiO_2$-Gly with sodium hypochlorite solution (Fig. 1).

2.7. Methods

Several methods were used for identification the structural properties for all prepared composite materials include: Fourier transform infrared spectroscopy (FTIR) for identification of the chemical structure of all materials. The thermal gravimetric analysis (TGA) provides valuable about the thermal stability of materials and the different weight ratios of all components. The structure texture properties of these materials were investigated by N2 adsorption-desorption isotherm using (BET) including the surface area and pore size and pore volume of all materials of concern. Scanning electron microscope (SEM) and transmission electron microscope (TEM) were used for determination of structural morphology of the composites and their elemental percentage composition. X-ray diffraction (XRD) was used to examine the crystal structure of the different nanocomposites and determination of their crystallite particle sizes. The x-ray photoelectron spectroscopy (XPS) provide valuable information about composition percentage of elements of different materials analysis were among the techniques used to analyze their structure.

2.8. Antibacterial activity tests

a) Disk diffusion assay

The antimicrobial activity for the synthesized nanocomposites were tested against *Escherichia coli* ATCC 26922, *Pseudomonas aeruginosa* ATCC 27853, *Bacillus stearothermophilus,* and *Staphylococcus aureus* ATCC 12228 using the well diffusion method. Mueller Hinton Agar (MHA) medium was used. The standardized culture of test bacteria was first evenly spread onto the surface of Mueller-Hinton agar plates using sterile cotton swabs. Four wells (7 mm) were made in each plate with a sterile corkborer. Wells were filled with 50 μL nanocomposites at 10 mg/mL concentration. In the fourth well, 50 μL of sterile distilled water (as a negative control) was added to each assay plate. 400 μL of dimethyl sulfoxide (DMSO) $(CH_3)_2SO$ was used as a solvent control. Levofloxacin disk (5 μg) was used as a positive control for Gram-negative bacteria. Amoxicillin disk (25 μg) was used as a positive control for Gram-positive bacteria. All the plates were then covered with lids and incubated at 37 °C for 24 h. The size of inhibition zones was measured, and the antimicrobial activity of the nanocomposites was expressed in terms of the average diameter of the inhibition zone in mm. The statistical analyses were used to calculate the needed statistical parameters: $\overline{X}$: Averge, SD: standard deviation, SE: standard error.

b) Microbroth dilution assay

The MIC, which refers to the lowest concentration of the drug/chemical that inhibits the growth of the test bacteria, can be determined using serial dilution methods. This procedure establishes the antibacterial concentrations that prevent bacteria growth
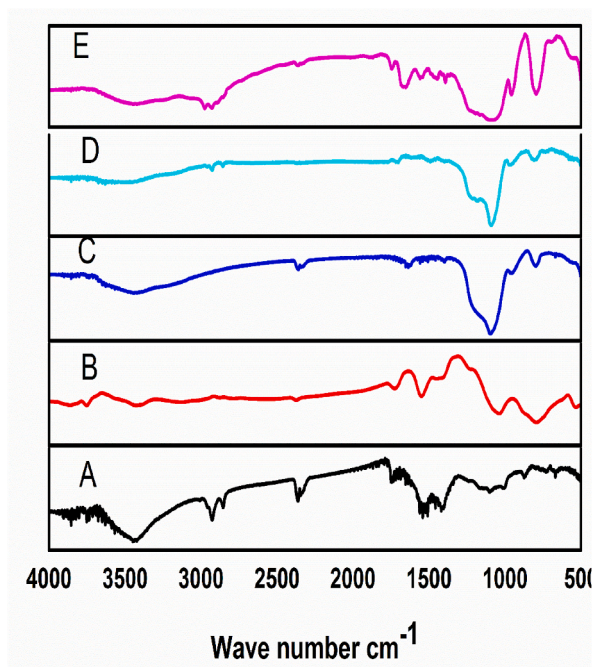
Fig. 2. FTIR spectra of A) AC, B) ZnO-NPs/AC, C) ZnO-NPs/AC@SiO$_2$,D) ZnO-NPs/AC@SiO$_2$@mSiO$_2$, E) ZnO-NPs@SiO$_2$@mSiO$_2$–Gly.

effectively and indicates the dosage that should be effective. A standardized microbial inoculum (compared to 0.5 MacFarland turbidity standard) is added to the wells containing serial dilutions of the test compounds, and the bacteria growth is monitored as a change in turbidity. Four titer plates indicated for bacteria were used.

For each 96 microtiters plate, wells 1–10 were used for nanocomposites that was serially diluted by two folds dilution using sterile nutrient broth, while wells 11 and 12 were used as negative and positive growth controls, respectively. A 25 µL of standardized test organism were added to each well. Plates were incubated for 24 h at 37 °C. The minimum inhibitory concentration (MIC) of the tested nanocomposite was calculated.

3. Results and discussion

3.1. Preparation

In this study, silica and mesoporous silica were used for coating the ZnO-NPs/AC nanocomposite. This would improve the ZnO-NPs/AC's mechanical and thermal properties [24] and increase the surface functionality of the silica or m-silica with antibacterial groups more useful. In this fabrication procedure, CTAB was employed to create m-silica, which increases the system's wettability and accessibility while also enhancing ZnO-NP dispersibility during the creation of the ZnO/AC@SiO2@mSiO2 nanocomposite [25]. The functionality of m-silica with N-halamine antibacterial groups on its surface is made possible by the presence of silanol groups, siloxane bridges hydroxyl groups on silica, or m-silica. In addition to providing ZnO-NPs with increased surface area, mesoporous silica also provides a method for functionalizing with N-halamine as an antibacterial.

3.2. FT-IR spectra

FT-IR spectra technique used to investigate the impregnation of ZnO-NPs onto the activated carbon(AC) and to examine its silica, mesoporous silica and functionalized glycinate coated materials: ZnO-NPs/AC@SiO$_2$, ZnO-NPs/AC@SiO$_2$@mSiO$_2$ and ZnO-NPs@SiO$_2$@mSiO$_2$-Gly (Fig. 2A–E). The FTIR spectrum of activated carbon AC (A) exhibits an absorption band at 3440 cm^{-1} due to the (O–H) stretching vibration of polymeric compounds groups. The peaks at 2924 and 2854 cm^{-1} are assigned due to the methylene hydrocarbon (C–H) stretching vibrations. The peak at 1456 cm^{-1} is assigned due to (C=C) stretching vibration of the activated carbon (AC). The bands observed at 1750 cm^{-1} are probably due to carbonyl C=O whereas, the bands at 1000 cm^{-1} is due to C–O stretching vibration. All these FT-IR assignments are based on FTIR results previously reported for similar materials [8,23,26]. The increase of adsorption of AC tendency towards the ZnO-NPs is probably due to the presence of functional groups of the activated carbon surface [21].

The FTIR spectra of silica or mesoporous silica and functionalized coated materials: ZnO-NPs/AC@SiO$_2$, ZnO-NPs/AC@SiO$_2$@mSiO$_2$ and ZnO-NPs@SiO$_2$@mSiO$_2$-Gly (Fig. 2C-E) showed three regions of absorptions. The first region at 3500–3200 cm^{-1} is assigned due to υ(O–H) or υ(N–H) stretching vibrations. The second region is observed at 1640-1750 cm^{-1}, which is assigned
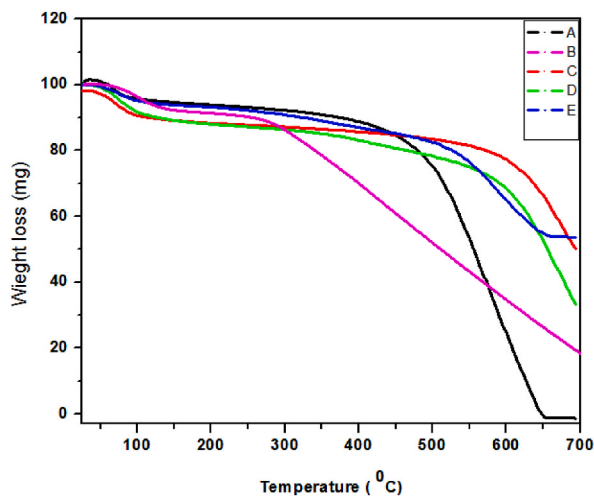
Fig. 3. TGA of A) AC, B) ZnO/AC, C) ZnO/AC@SiO$_2$, D) ZnO/AC@SiO$_2$@mSiO$_2$, E) ZnO@SiO$_2$@mSiO$_2$–Gly.

Table:1
weight ratio of ZnO/AC.

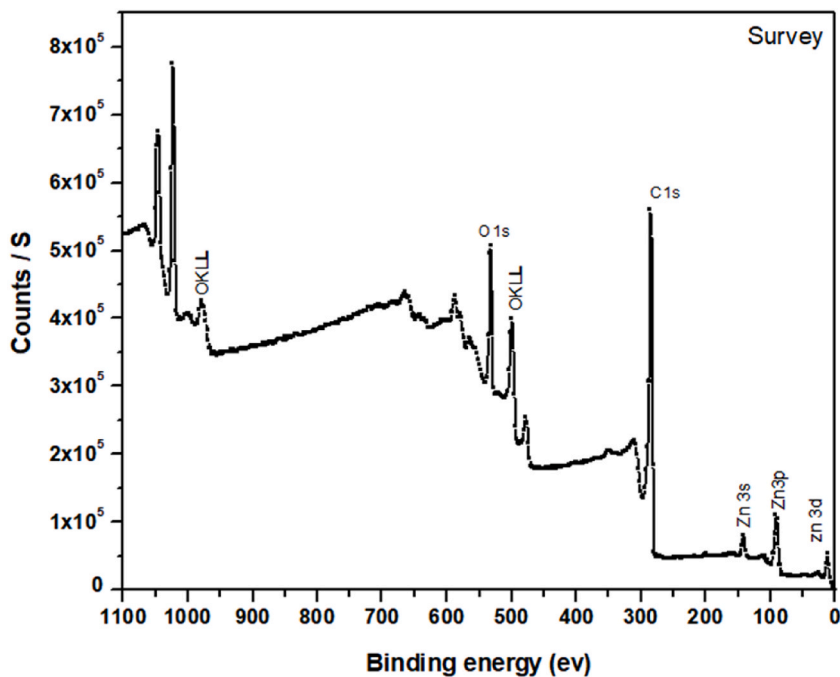| Material	ZnO/AC wt. ratio
ZnO-NPs/AC	20/80
ZnO-NPs/AC@SiO$_2$	20/50
ZnO-NPs/AC@SiO$_2$@mSiO$_2$	20/40
ZnO-NPs/AC@SiO$_2$@mSiO$_2$-N-Gly	20/38

Fig. 4. XPS survey spectrum for ZnO-NPs/AC material.

due to stretching vibration of υ(CO) at 1750 cm^{-1} and at 1670 and 1640 cm^{-1} due to bending vibrations of σ(N–H) and σ(OH) vibrations, respectively. The third region of absorptions showed peaks at 1095 cm^{-1}, 807 cm^{-1}, and 471 cm^{-1} cm^{-1}are assigned due to symmetrical and asymmetrical υ(Si–O) vibrations [9,10,23,26]. The peak or shoulder at 967 cm^{-1} is assign to the tensile vibration of

Table 2
XPS Elemental corelines and its percentages (%) composition of ZnO-NPs/AC.

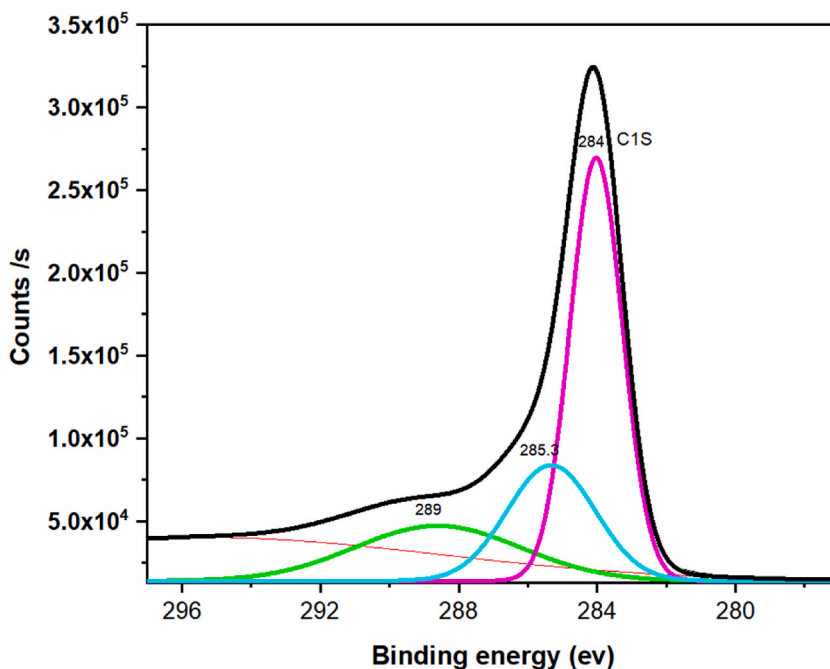| Element (coreline)	Atomic (%)
C1S (284eV)	82.33
N1S (400eV)	0.83
O1S (532eV)	14.52
Zn2p3(1022eV)	2.32

Fig. 5. Fitted C1s XPS core level spectrum of ZnO-NPs/AC material.

Si–OH [9,10,23,26]. The absence of peaks due to Zn–O vibrations is due to its low content of Zn–O and is probably obscured with the high intensity peaks of silica or AC.

3.3. Thermogravimetric analysis

Thermogravimetric analysis (TGA) for AC, ZnO-NPs/AC, ZnO-NPs/AC@SiO$_2$, ZnO-NPs/AC@SiO$_2$@mSiO$_2$ and ZnO-NPs@SiO2@mSiO$_2$–Gly materials were examined at 20–750 °C (Fig. 3A–E). There was gradual weight loss for these samples as the temperature increases. The first step of weight loss occurs at <100 °C is probably due to loss of solvents e.g. water or ethanol from the nanocomposites. The second step of weight loss occurs at 100–350 °C, which is probably due to a gradual loss of carbon from the back bone of AC as well as loss of water from a dihydroxylation and condensation of silica-silanol groups, [8,10,11,23,27]. The third step occurs at > 350 °C is probably due to the decomposition of all carbon of AC as well as decomposition of the glycinate or *N*-halamine glycinate functional group attached to the m-silica [8–11]. At temperatures between 25 and 750 °C, the pristine AC material loses around 98 % of its total weight. The remaining 2 % residue (Fig. 3A) is likely contained residue of the AC material's constituents. The TGA of ZnO-NPs/AC nanocomposite the weight loss drops from 100 % to 20 % (Fig. 3B) with weight ratio of ZnO/AC = 20/80. The TGA of ZnO-NPs/AC@SiO$_2$ nanocomposite, the weight loss drops from 100 % to ca. 92 % due to loss of adsorbed H$_2$O, the second step start at high temperature ca. 600 °C due loss of 42 % AC) (Fig. 3C) for ZnO-NPs/AC@SiO$_2$ nanocomposite. This is probably due to presence of (ZnO + SiO$_2$) (Fig. 3C) with weight ratio (ZnO + SiO$_2$)/AC + H$_2$O = 50/50. The presence of SiO$_2$ showed a strong thermal stabilization of the system (Fig. 3). The weight loss of AC (%) for The TGA of ZnO-NPs/AC@SiO2@mSiO2 composite material (Fig. 3D) showed a drop from 100 % to 40 %. In the first stage at 100C, there is a loss of absorbed water of ca. 8 % adsorbed water. In the second stage from 100 to 550C, this is loss of (AC + H2O) of 32 %. Due to presence (ZnO-NPs + SiO2+mSiO2) (Fig, 3D) the weight ratio (ZnO + SiO$_2$+MSiO$_2$)/(AC + Total H$_2$O) = 60/40, where ca.10 % of the composite material is m-silica. The glycinate functional groups in the study were related with a modest increase in total weight reduction.

A slight increase in total weight loss was associated with the glycinate functional groups in the functionalized material ZnO-NPs@SiO$_2$@mSiO$_2$-Gly (Fig. 3E). In preparation section: ZnO-NPs/AC@SiO2, ZnO-NPs/AC@SiO2@mSiO2 and ZnO-NPs/
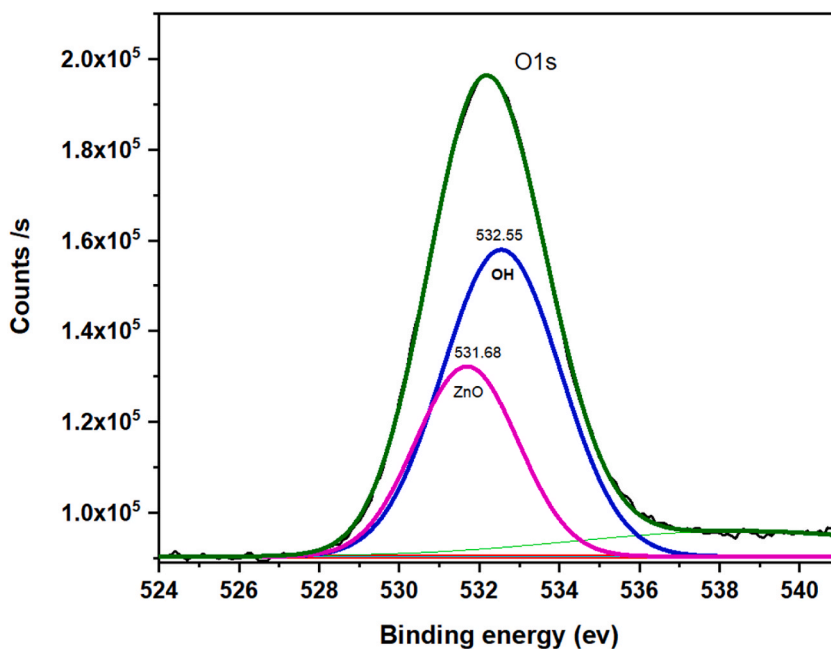
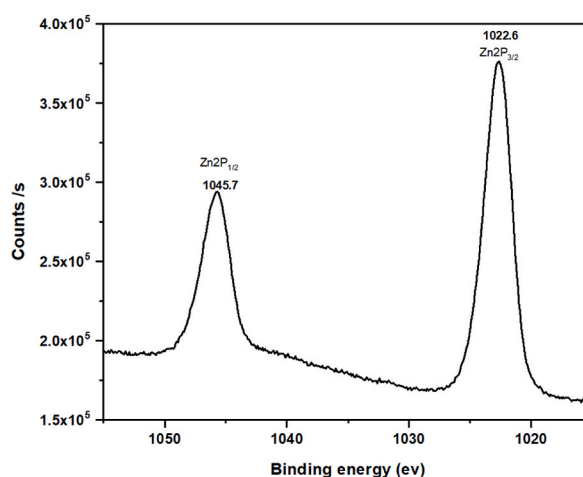**Fig. 6.** Fitted O1s XPS core level spectrum of ZnO-NPs/AC material.

Fig. 7. Fitted Zn2p XPS core level spectrum of ZnO-NPs/AC material.

AC@SiO2@mSiO2-N-Gly, the percentage weight ratio of AC and ZnO were given in Table 1. The TGA analysis is based on similar reported results [10,11]. From the TGA results, the percentage weight ratio of ZnO/AC was calculated for these materials as given follow.

The percentage wt. ratio decreases from the order from 0.25 to 0.4 for ZnO-NPs/AC@SiO$_2$ and to 0.5 for ZnO-NPs/AC@SiO$_2$@mSiO$_2$ and to 0.52 for ZnO-NPs/AC@SiO$_2$@mSiO$_2$-glycinate.

3.4. XPS results

The XPS survey spectrum of ZnO-NPs/AC is exhibited in Fig. 4. The survey spectrum showed peaks at 285, 400, 532 and 1022 eV corresponding to C1s, N1s, O1s and Zn2P, respectively [21,28]. The atomic percentages of all elements and their corresponding core-line binding energies (BE's) are given in Table 2. The XPS survey spectrum of ZnO-NPs/AC (Fig. 4) showed the highest intensity peak of carbon centered at 285 eV of C1s core, due to the presence of activated carbon precursor. This is clearly confirmed from the SEM images (Fig. 8 (a&b). The survey spectrum of ZnO-NPs/AC reveals the presence of four O1s peaks, one is associated with zinc oxide ZnO-NPs at ca. 532 eV and three oxygen-containing functional states at 500–650 eV. These states were assigned for hydroxyls
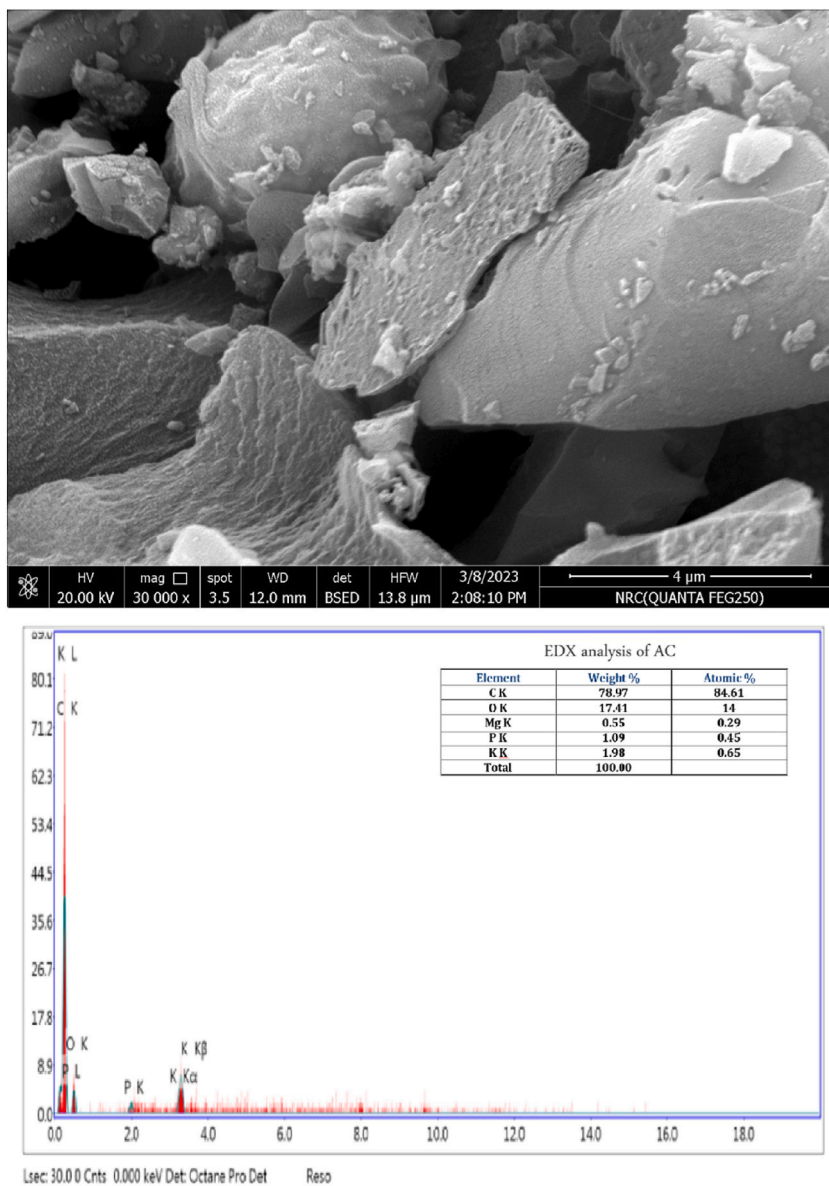
EDX analysis of AC		
Element	Weight %	Atomic %
C K	78.97	84.61
O K	17.41	14
Mg K	0.55	0.29
P K	1.09	0.45
K K	1.98	0.65
Total	100.00	

Lsec: 30.0 0 Cnts 0.000 keV Det: Octane Pro Det   Reso

Fig. 8. SEM-image and EDX data of AC.

(OH), ethers (C–O), carbonyls (C=O) and carboxylic acids (O–C=O) [21,24,29]. The doublet peaks at binding energy at 1020–1060 eV are associated with the presence of Zn2P core [8]. The observed low energy peaks at 50–150 eV are probably corresponded to Zn LMM auger peaks [24,28].

The carbon C1s spectrum peak is fitted with presence of three signals centered at 284.99, 286.54 and 289.04 eV corresponding to three components of carbons: C–C/C–H, C–N/C–O and COOH/COOR (Fig. 5 showed) [21,28].

The oxygen O1s spectrum peak appearing at around 532 eV (Fig. 6) is fitted with presence of two components at 531.7 and 532.5 eV due to the O^{2-} ion of Zn–O and OH species, respectively [21,28].

XPS of ZnO-NPs/AC nanocomposite confirmed the formation of ZnO-NPs, which are impregnated onto AC. Fig. 7 showed the core level scan spectrum of Zn2p. It showed a doublet of peaks centered at ~1022 ± 0.1 eV and ~1045 ± 0.1 eV corresponding to the two components Zn2p3/2 and Zn2p1/2, respectively. The energy gap between Zn 2p3/2 and Zn 2p1/2 has the same value of 23 eV as that reported in literature [8,21,28].

3.4.1. Scanning electron microscopy (SEM)

The SEM images morphology and its energy dispersive X-ray microscopy (EDX) of blank AC and that of ZnO-NPs/AC nano-composite are shown in Figs. 8 and 9. The SEM image of the blank AC shows rough surfaces with fused carbon layers (Fig. 8). EDX
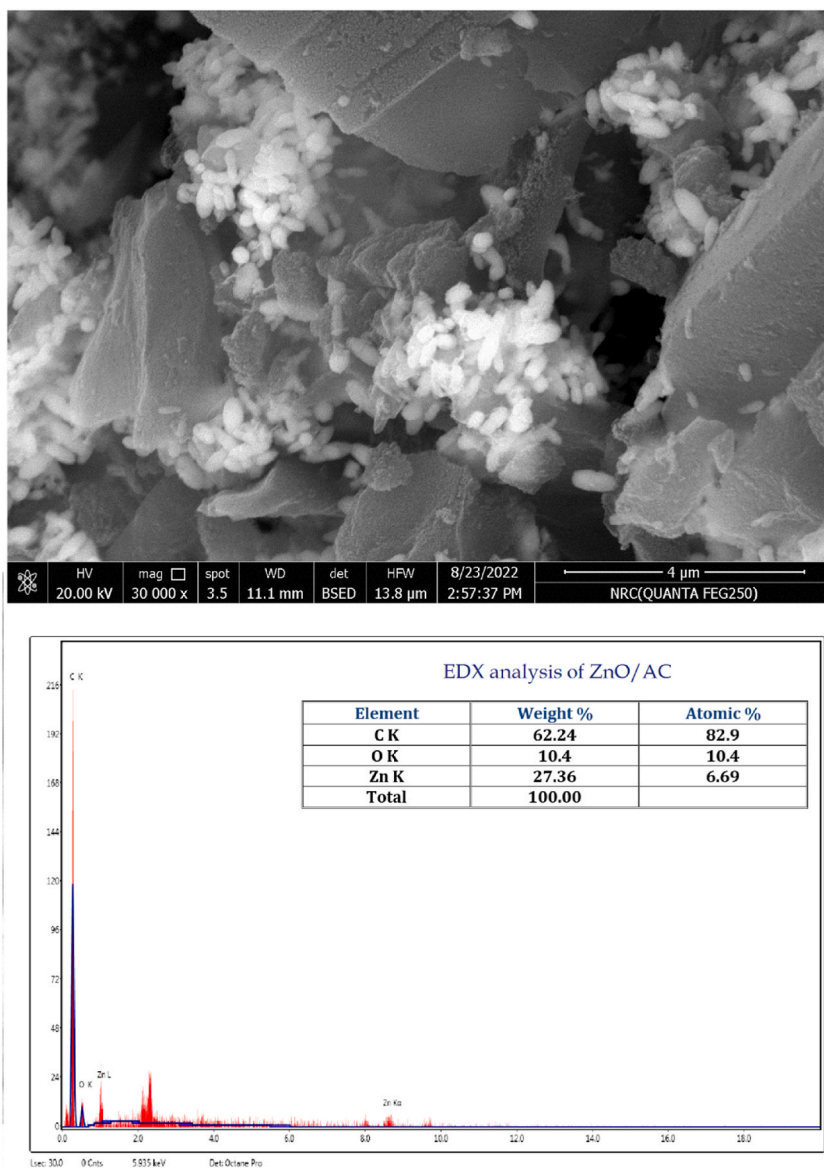
Fig. 9. SEM-image and EDX data of ZnO-NPs/AC.

results showed high content of carbon (78.9 %), low content of oxygen (17.4 %) and traces of other elements (Fig. 8). The SEM-image of ZnO-NPs/AC nanocomposite after introduction of ZnO-NPs into AC exhibits more smooth surfaces (Fig. 9) [8,27,30,31]. The introduction of ZnO into activated carbon was evident from EDX analysis of ZnO-NPs/AC which showed the presence of 27.4 % for Zn and reduction of both C% from 78.9 % to 62.2 % and of O % from 17.4 % to 10.4 %. Similar results were also reached from the TGA analysis discussed in TGA section. SEM image of ZnO-NPs/AC nanocomposite showed that ZnO-NPs are well impregnated into the surface of activated carbon. There is some agglomeration of ZnO-NPs into the surface cavities of AC. This is probably due to its high polarity or electrostatic attraction between the ZnO-NPs and AC [8,28,31]. The morphology of ZnO-NPs is seen as bullets-like shape forming flower petals-shaped morphology or decorated the surface of AC (Fig. 9).

The SEM-image of silica coated ZnO-NPs/AC@SiO$_2$ nanocomposite material (Fig. 10) showed that the ZnO-NPs/AC composites are well coated by SiO$_2$ of spherical particles, where the ZnO-NPs were well coated with silica and these nanoparticles could be seen underneath the coating SiO$_2$ layers. The presence of silica (SiO$_2$) coated layer was evident from the EDX results. It showed the presence of 16.79 % of silicon and a considerable decrease of zinc % and carbon % contents in comparison with that of ZnO-NPs/AC (Fig. 9). The silica coating with AC material is probably occurred due to condensation between the OH groups of zinc oxide with carboxylic acid or ester of AC.

When a mesoporous silica (mSiO$_2$) coating layer was added onto the silica (SiO$_2$) coated layer for ZnO/AC@SiO$_2$@mSiO$_2$ nano-composite. This is probably form by Vander Wall's force or the cross-linking of siloxane networks. This was evident from SEM-image
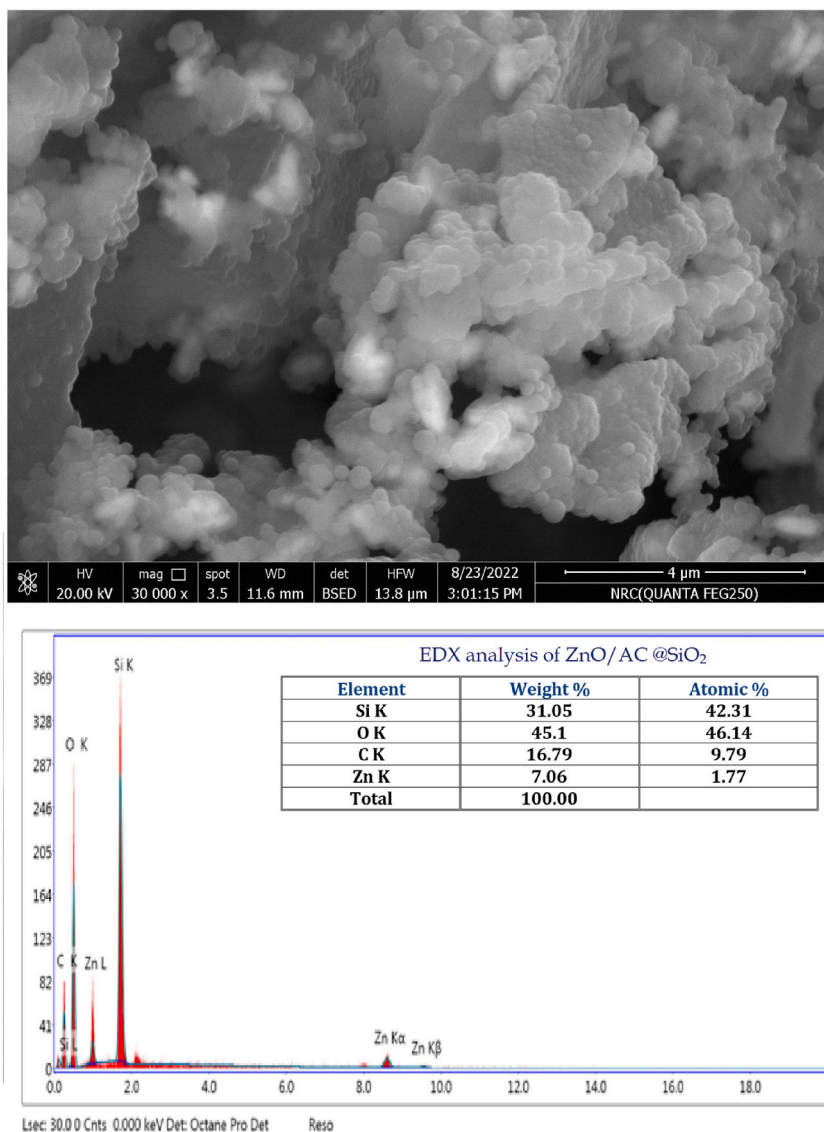
Fig. 10. SEM-image and EDX data of ZnO-NPs/AC@SiO$_2$.

(Fig. 11). The coating with m-silica was evident from EDX analysis, where silicon content has increased from 30 % to 50 % and the content of Zn has decreased 7.0 %–2.44 %. The increasing of carbon content for ZnO-NPs/AC@SiO$_2$@mSiO$_2$ is probably due presence of unhydrolyzed alkoxy (OR) groups.

The SEM-image of ZnO-NPs@SiO$_2$@mSiO$_2$-Gly nanocomposite (Fig. 12) displays agglomerated stacks of silica spheres of nanocomposites due to physical electrostatic attraction after removal of activated carbon plates. After functionalization with glycinate silane agent (Gly-S). The surface coating of ZnO-NPs@SiO$_2$@mSiO$_2$ with glycinate silane agent was evident by of presence of carbon, amine nitrogen and high content of hydrogen (Fig. 12).

3.5. TEM analysis

Transmission electron microscopy (TEM) was conducted to investigate the morphology and microstructure of the AC, ZnO-NPs/AC nanocomposite and its coated silica-, mesoporous-silica and functionalized glycinate nanocomposite materials [10,11]. The typical TEM image of pristine AC given in Fig. 13a indicates that the activated carbon (AC) consists of grey color layers or sheets of carbons. The TEM-image of ZnO-NPs/AC nanocomposite (Fig. 13b) exhibits a disordered worm-like shape of mesoporous structure, where the ZnO-NPs are occupied the pores of AC as black particles.

TEM-image of silica coated nanocomposite (ZnO-NPs/AC@SiO$_2$) exhibits the agglomeration of silica (SiO$_2$) nanospheres of different particle sizes coated onto the surface of AC(Fig. 14a). The TEM-image of mesoporous coated nanocomposite (ZnO-NPs/
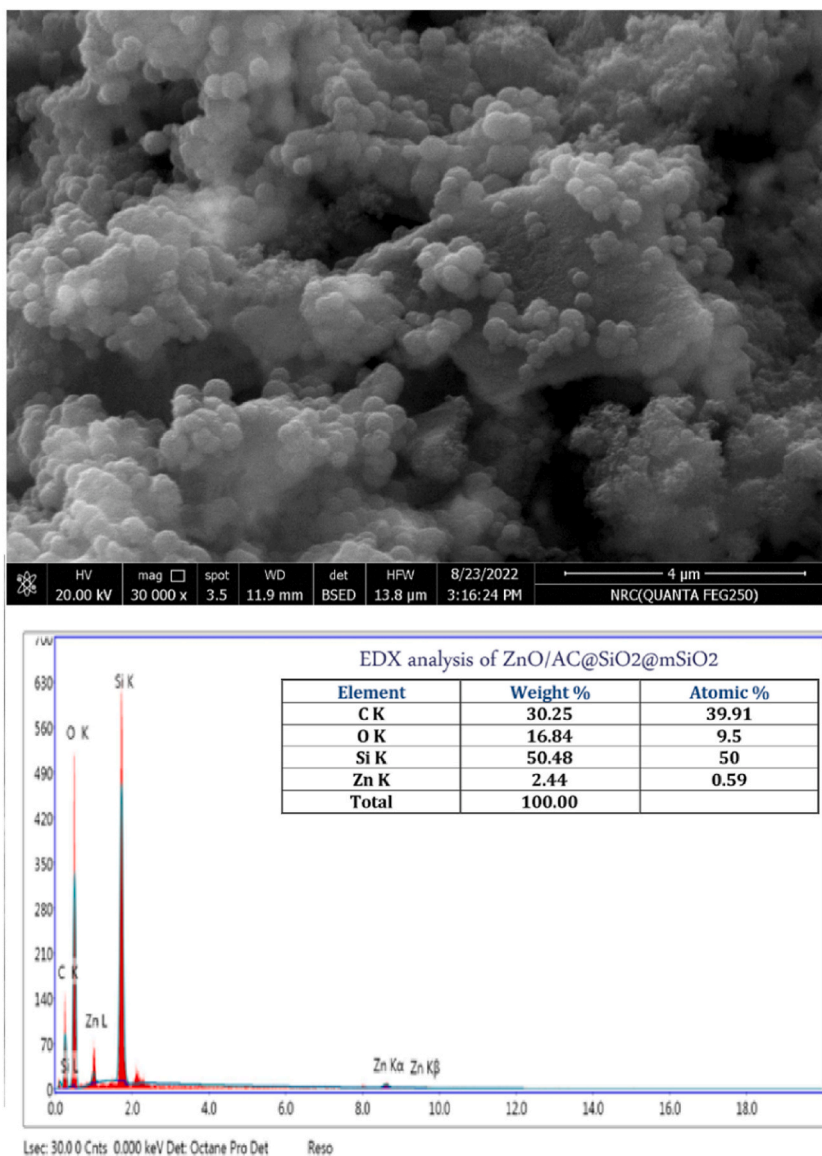
EDX analysis of ZnO/AC@SiO$_2$@mSiO$_2$		
Element	**Weight %**	**Atomic %**
C K	30.25	39.91
O K	16.84	9.5
Si K	50.48	50
Zn K	2.44	0.59
Total	100.00	

Fig. 11. SEM and EDX data of ZnO-NPs/AC@SiO$_2$@mSiO$_2$.

AC@SiO$_2$@mSiO$_2$) showed that the silica nanosphers SiO$_2$ are coated with a worm like mesoporous silica thin layers with presence of ZnO-NPS of 9–14 nm dispersed into the pores as dark nanoparticles (Fig. 14b). The TEM-image of ZnO-NPs@SiO$_2$@mSiO$_2$-Gly nanocomposite showed that the silica nanosphers SiO$_2$ are coated with mesoporous silica and glycinate functional group (Fig. 15)

3.6. BET analysis

BET analysis of ZnO-NPs/AC, ZnO-NPs/AC@SiO$_2$, ZnO-NPs/AC @SiO$_2$@mSiO$_2$, ZnO-NPs@SiO$_2$@mSiO$_2$-Gly nanocomposites were investigated by N$_2$ sorption-desorption isotherm. The texture results of these materials including surface area, pore size and pore volume are analyzed for these materials and summarized in Table 3. The impregnation of ZnO-NPs onto the AC surface contributes to slight decrease the surface area from 810 m^2/g to 772 m^2/g (Table 3) [30,31]. After templating with ZnO-NPs/AC nanocomposite with silica spheres layer (SiO$_2$), the surface area has significantly decreased to ca. 282 m^2/g. This is probably due to formation of silica layers onto the ZnO-NPs/AC nanocomposite. The surface area was further decreased to ca. 139 m^2/g upon coating with mesoporous layer (mSiO$_2$) and to 15.0 m^2/g after functionalization with glycinate silane (Table 3).
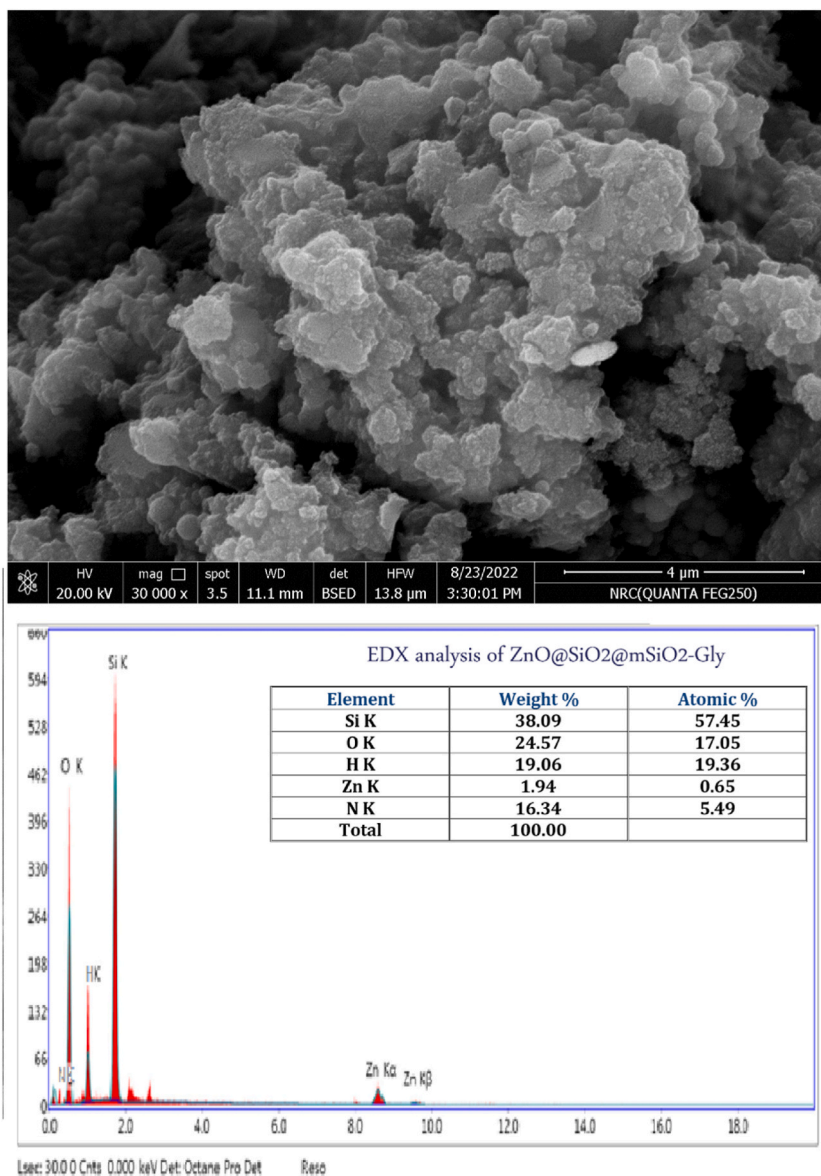
Fig. 12. SEM and EDX data of ZnO-NPs@SiO$_2$@mSiO$_2$-Gly.

3.7. X-ray diffraction (XRD)

The XRD analysis for ZnO-NPs/AC, ZnO-NPs/AC@SiO$_2$, ZnO-NPs/AC@SiO$_2$@mSiO$_2$ and ZnO-NPs@SiO2@mSiO$_2$–Gly materials were examined, the XRD patterns are given in Fig. 16 (A-D). The XRD patterns of the tested samples matched well with that of pure ZnO [8,21,28,31,32]. The XRD patterns of these materials have showed that the all-characteristic peaks labeled of (*) are for wurtzite hexagonal ZnO NPs according to the JCPDS (36–1451) were indexed at 31.74°, 34.39°, 36.24°, 47.58°, 56.58°, 62.87°, 66.31°, 67.89°, 69.07°, 72.45° and 76.86° with no impurities [20,21]. It is obvious that these XRD characteristic peaks become slightly broader after coating with silica or mesoporous silica. This results of slight a decrease of particle size of ZnO-NPs in comparison with uncoated material ZnO-NPs/AC (Table 4). The broad two peaks labeled as ($) at 22° and 44° were assigned correspond to the AC substrate [8,21,28,32]. The absence of impurities peaks may indicate that the final material was a combination of ZnO and AC with high purity. The crystallite size of the crystals was calculated using Scherrer's formula (1).

$$D = 0.9\lambda \ / \ (\beta \cos \Theta) \tag{1}$$

Where D is the diameter of the crystallites of the crystals, λ is the wavelength of the CuKα line (0.15406 nm), β is the full width at half maximum (FWHM) in radians, and Θ is the Bragg angle. The crystallite particle sizes of ZnO-NPs in the different materials are listed in
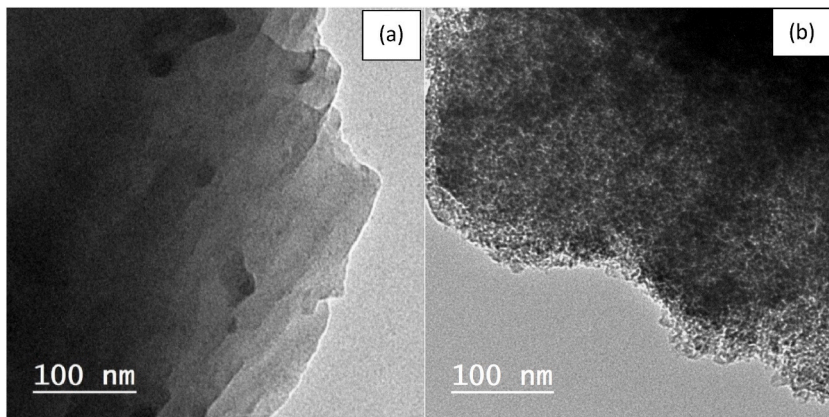
Fig. 13. TEM image of (a) pristine AC, (b) ZnO-NPs/AC nanocomposites.
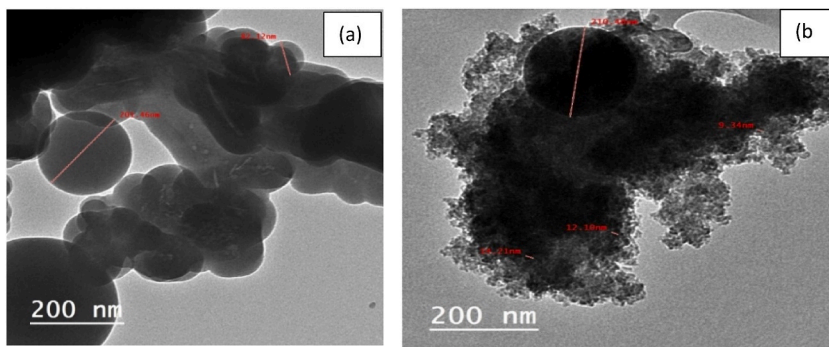

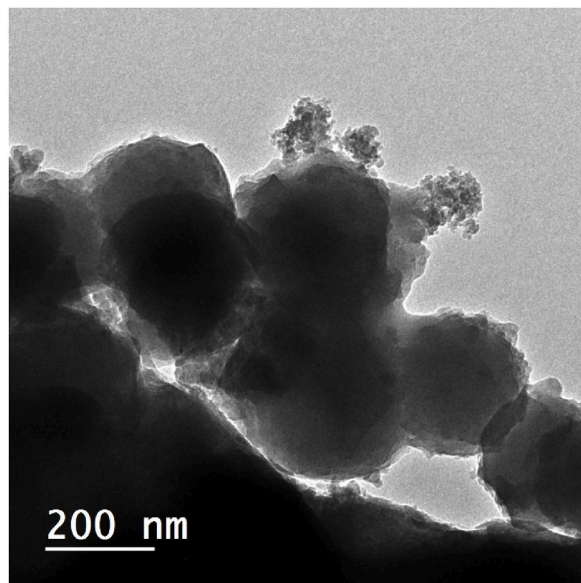**Fig. 14.** TEM image of (a) ZnO-NPs/AC@SiO$_2$, (b) ZnO-NPs/AC@mSiO$_2$.
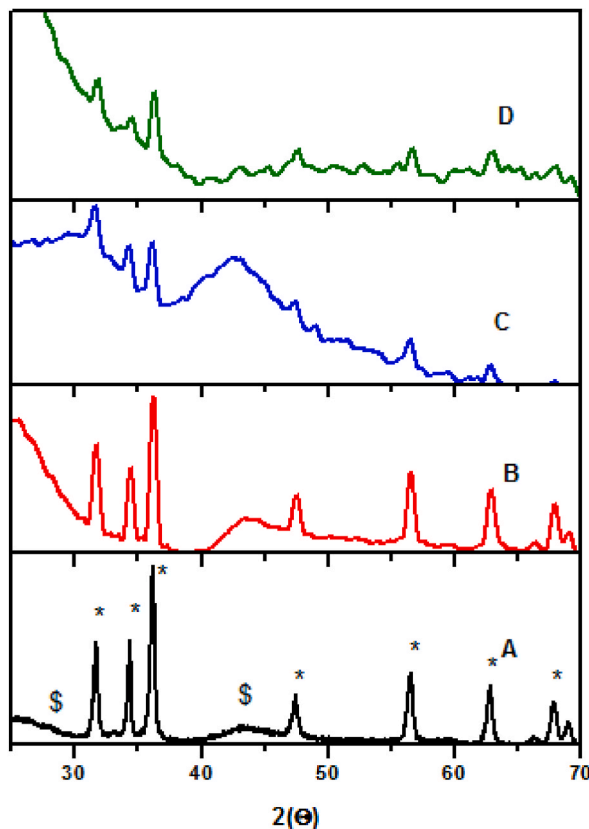

Fig. 15. TEM image of ZnO-NPs@SiO$_2$@mSiO$_2$-Gly nanocomposite.

Table 3
Texture and structure parameters of nanocomposites at 150 °C for 4 h.

Material	Pore size(A)	S_{BET} (m^2/g)	V(p)(cc/g)
AC	–	800	–
ZnO-NPs/AC	1.78	773	0.370
ZnO-NPs/AC@SiO$_2$	1.69	283	0.134
ZnO-NPs/AC@SiO$_2$@mSiO$_2$	1.78	139	0.064
ZnO-NPs@SiO$_2$@mSiO$_2$-Gly	2.65	15.0	0.006

Fig. 16. XRD patterns of the (A) ZnO-NPs/AC, (B) ZnO-NPs/AC@SiO$_2$, (C) ZnO-NPs/AC@SiO$_2$@mSiO$_2$, (D) ZnO-NPs@SiO$_2$@mSiO$_2$-Gly.

Table 4
Crystallize particle sizes of ZnO-NPs in the different materials.

System	Particle size(nm)
ZnO-NPs/AC	17.46
ZnO-NPs/AC@SiO$_2$	12.87
ZnO-NPs/AC@SiO$_2$@mSiO$_2$	12.80
ZnO-NPs@SiO$_2$@mSiO$_2$-Gly	12.84

Table 4. There is slight decreasing from the parent ZnO/AC after coating with silica precursors. The crystallite particle sizes obtained from XRD analysis using Scherrer's formula (Table 4) are closed to the data obtained from TEM analysis for ZnO-NPs/AC@SiO$_2$@mSiO$_2$ nanocomposite (Fig. 14).

3.8. Antibacterial activities of nanocomposites

3.8.1. The well-diffusion method

The well-diffusion method is a method typically used to evaluate the antimicrobial effects of variety of AC, ZnO-NPs/AC, ZnO-NPs/AC@SiO$_2$, ZnO-NPs@SiO$_2$@mSiO$_2$, ZnO-NPs@SiO$_2$@mSiO$_2$-N-halamine glycinate substances. The antimicrobial activity results using
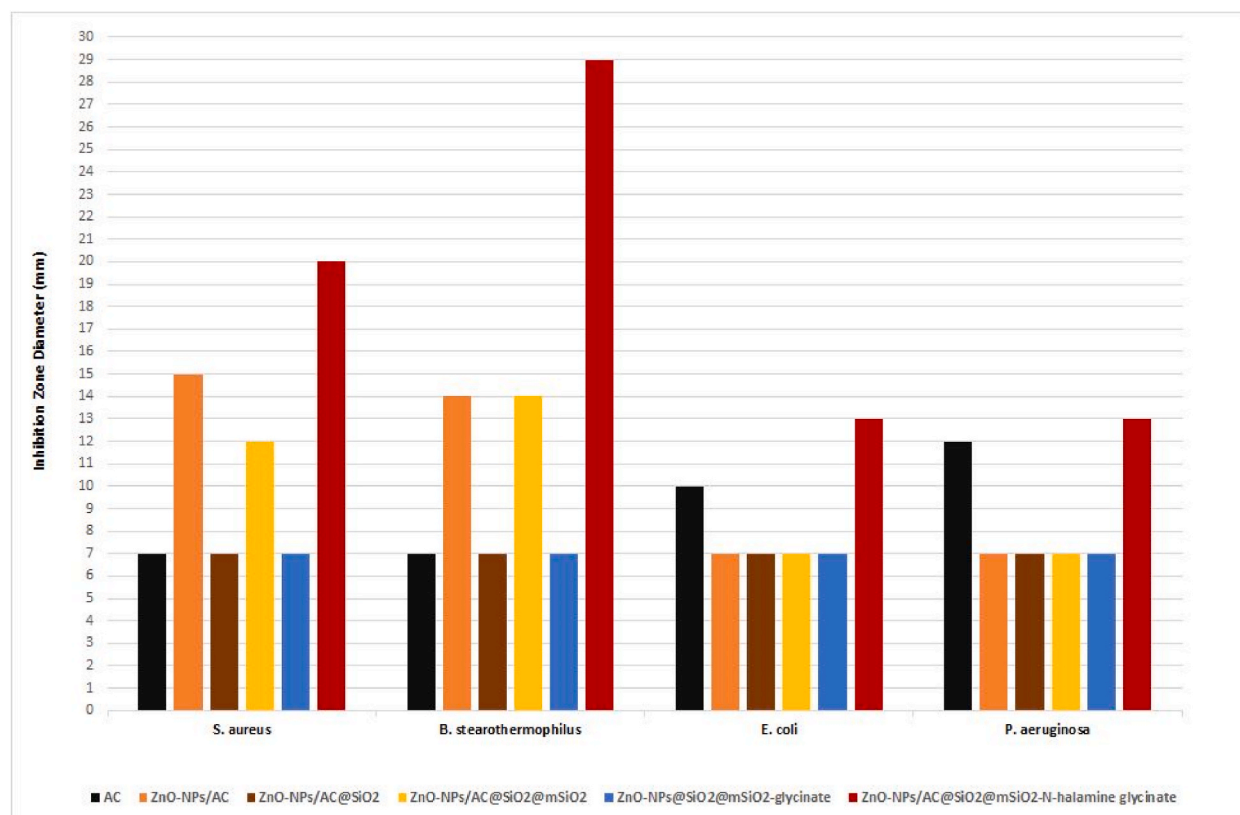
Fig. 17. Antibacterial activities of nanocomposites by agar well diffusion method.

the well-diffusion method of the nanocomposites against two Gram-positive and two Gram-negative bacteria are depicted in Fig. 17 and Table 5. All antibacterial zone inhibition plates are provided in the sublementary file. It is found that the pristine AC showed no antibacterial activities towards Gram-positive bacteria but it showed slight positive antibacteria activity for Gram-negative bacteria. The nanocomposites materials demonstrated different antibacterial activities against all four bacterial species with larger inhibition zones for the Gram-positive bacteria than that of the Gram-negative bacteria. In the case of Gram-positive bacteria, the highest antibacterial activity was for ZnO-NPs@SiO$_2$@mSiO$_2$-*N*-halamine-Gly followed by ZnO-NPs/AC and ZnO-NPs/AC@SiO$_2$@mSiO$_2$. This behavior is propably refers to two factors, the diffusion factor in case mesoporous silica (mSiO$_2$) and the presence of antimicrobial agents: N-halamine functional group and ZnO-NPs. There is no antimicrobial activity in case of ZnO-NPs@SiO$_2$ and ZnO-NPs@SiO$_2$@mSiO$_2$-Gly due to absence of mesoporous silica in the first material and absence of N-halamine functional in the second material.

The low antibacterial activity of the Gram-negative bacteria is due to the complexity cell wall, which contains an outer membrane that serves as a barrier and makes it more difficult for antimicrobial drugs to enter while having a thinner peptidoglycan layer, may be the cause of this behavior [31–33]. With the exception of *E. coli*, the ZnO-NPs@SiO$_2$@mSiO$_2$-*N*-halamine-Gly nanocomposite material had the highest zones of inhibition. See suplementary file. The ZnO-NPs@SiO$_2$@mSiO$_2$-N-halamine-Gly nanocomposite has two antimicrobial centers (ZnO-NPs and -*N*-halamine-Gly) are likely to blame for this behavior. These nanocomposites are probably produce ROS, which results in cell damage [32]. That of course could caused of disrupt some bacterial cell essential functions and cause death.

3.8.2. The minimal inhibitory concentration (MIC)

The minimal inhibitory concentration (MIC) results of the powders: AC, ZnO-NPs/AC, ZnO-NPs/AC@SiO$_2$, ZnO-NPs@SiO$_2$@m-SiO$_2$, and ZnO-NPs@SiO$_2$@mSiO$_2$-N-halamine glycinate are displyed in Fig. 18 and Table 6. Serial diluted concentrations (2 g/mL, 4 g/mL, 6 g/mL, 8 g/mL, and 10 g/mL) for control against 2 g-positive and 2 g-negative species. The results showed substantial MIC values lie between 3 and 10 g/mL. It showed that the MIC for Gram-positive *S. aureus* is lower than the MIC for Gram-negative *P. aeruginosa*. This is perhaps due to the ability of Gram-negative bacteria to create specific compounds that enhanced their resistance to oxidative stress. Similar research results on Gram-positive and Gram-negative bacteria have already been reported previously [31,32,34]. The antibacterial action of ZnO-NPs is achieved by a variety of processes, one of which is the formation of reactive oxygen species (ROS) within the cell. The other one is that ZnO-NPs can cause cell death by the release of excess of Zn^{2+} ions which causes a change in cellular metabolism. All the following types of bacteria including: *S. aureus, S. epidermidis, Streptococcus pyogenes,*

Table 5
Statistical Results of Zone inhibition of 2 g-positive and 2 g-negative bacterial strains.

Nanocomposite	Zone of inhibition (mm) Trials number			Statistical results		
	1	2	3	$\overline{X}$	SD	SE
S. aureus						
AC	7.00	7.00	7.00	**7.00**	**0.00**	**0.00**
ZnO-NPs/AC	15.00	14.80	15.20	**15.00**	**0.20**	**0.12**
ZnO-NPs/AC@SiO$_2$	7.00	7.00	7.00	**7.00**	**0.00**	**0.00**
ZnO-NPs/AC @SiO$_2$@ mSiO$_2$	11.90	11.90	12.20	**12.00**	**0.17**	**0.10**
ZnO-NPs@SiO$_2$@mSiO$_2$-Gly	7.00	7.00	7.00	**7.00**	**0.00**	**0.00**
ZnO-NPs@SiO2@mSiO2-N-halamine glycinate	19.70	19.90	20.40	**20.00**	**0.36**	**0.21**
B. stearothermophilus						
AC	7.00	7.00	7.00	**7.00**	**0.00**	**0.00**
ZnO-NPs/AC	14.00	13.80	14.20	**14.00**	**0.20**	**0.12**
ZnO-NPs/AC@SiO$_2$	7.00	7.00	7.00	**7.00**	**0.00**	**0.00**
ZnO-NPs/AC @SiO$_2$@ mSiO$_2$	13.90	13.90	14.20	**14.00**	**0.17**	**0.10**
ZnO-NPs@SiO$_2$@mSiO$_2$-Gly	7.00	7.00	7.00	**7.00**	**0.00**	**0.00**
ZnO-NPs@SiO2@mSiO2-N-halamine glycinate	28.80	29.00	29.20	**29.00**	**0.20**	**0.12**
E. coli						
AC	9.90	10.10	10.00	**10.00**	**0.10**	**0.06**
ZnO-NPs/AC	7.00	7.00	7.00	**7.00**	**0.00**	**0.00**
ZnO-NPs/AC@SiO$_2$	7.00	7.00	7.00	**7.00**	**0.00**	**0.00**
ZnO-NPs/AC @SiO$_2$@ mSiO$_2$	7.00	7.00	7.00	**7.00**	**0.00**	**0.00**
ZnO-NPs@SiO$_2$@mSiO$_2$-Gly	7.00	7.00	7.00	**7.00**	**0.00**	**0.00**
ZnO-NPs@SiO2@mSiO2-N-halamine glycinate	13.00	12.70	13.30	**13.00**	**0.30**	**0.17**
P. aeruginosa						
AC	11.90	12.10	12.00	**12.00**	**0.10**	**0.06**
ZnO-NPs/AC	7.00	7.00	7.00	**7.00**	**0.00**	**0.00**
ZnO-NPs/AC@SiO$_2$	7.00	7.00	7.00	**7.00**	**0.00**	**0.00**
ZnO-NPs/AC @SiO$_2$@ mSiO$_2$	7.00	7.00	7.00	**7.00**	**0.00**	**0.00**
ZnO-NPs@SiO$_2$@mSiO$_2$-Gly	7.00	7.00	7.00	**7.00**	**0.00**	**0.00**
ZnO-NPs@SiO2@mSiO2-N-halamine glycinate	13.00	12.70	13.30	**13.00**	**0.30**	**0.17**

Enterococcus faecalis, Bacillus subtilis, Escherichia coli, and *Klebsiella pneumonia* have been documented to be vulnerable to ZnO-NPs. Therefore, the ZnO-NPs material. very useful [31]. The microbiological results showed different MICs between gram-negative and gram-positive bacteria. The MICs were significantly lower for *E. coli*, resulting in susceptible profiles only for *Pseudomonas* strains. Nanoparticles have unique physicochemical properties that make these materials have novel antibacterial mechanisms of action. These nanomaterials have various effects on microbes, depending on their unique structure and size. The shape and particle size play an important effect on their antimicrobial activity e.g. rod-like ZnO-NPs exceed plate-like nanoparticles in antimicrobial activity. Nanoparticles are promising antimicrobials today due to their antibacterial and antiviral actions. They have showed more effective antibacterial to combat bacteria than traditional antibiotics [32,33].

Despite the fact that the MIC test provides a quantitative measurement of the antimicrobial agent's efficacy, the well diffusion method offers a qualitative assessment. The two methods offer complete assessment of the antimicrobial activity of a particular agent against a specific microorganism [35]. The well-diffusion method is more sensitive to the diffusion rate of the antimicrobial agent. The diffusion rate is dependent more on the diffusion rate of the antimicrobial agent through agar. This is dependent on the agent's physicochemical properties, such its solubility. The zone of inhibition is dependent on the diffusion rate is slow, even though the MIC of the agent is low [36]. Despite the fact that the MIC test is considered to be more accurate than the well diffusion method, the well diffusion method is more convenient and can be used to screen a larger number of antimicrobial agents [37].

3.8.3. Mechanism of antibacterial activity

The release of generated of H_2O_2 from treatment of pollutant water with using one of the prepared nanocomposites as a chemical species that has effective for antibacterial action as previously reported of similar systems [38,39]. The relatively permeable cell membrane for H_2O_2 could be easily damaged the bacterial cell by the penetration of H_2O_2 released from ZnO-NPs species (Fig. 19). Xiaoling Xu et al. [40] have proposed that the presence of oxygen vacancies on the ZnO surface act as a key factor for the production of the H_2O_2.

4. Conclusions

A well design antibacterial nanocomposite material ZnO-NPs@SiO$_2$@mSiO$_2$-*N*-halamine-Gly was achieved. Zinc oxide nanoparticles (ZnO-NPs) were firstly impregnated into activated carbon (AC) to form ZnO-NPs/AC nanocomposite. Silica and mesoporous silica coated nanocomposite materials (ZnO-NPs/AC@SiO$_2$, ZnO-NPs/AC@SiO$_2$@mSiO$_2$) were performed by coating the surface of ZnO/AC nanocomposite with silica (SiO$_2$) and mesoporous silica (mSiO$_2$) through sol-gel process. The *N*-halamine glycinate nanocomposite (ZnO-NPs@SiO$_2$@mSiO$_2$-*N*-halamine-Gly) was then prepared throughout functionalization of ZnO-NPs@SiO$_2$@mSiO$_2$ with
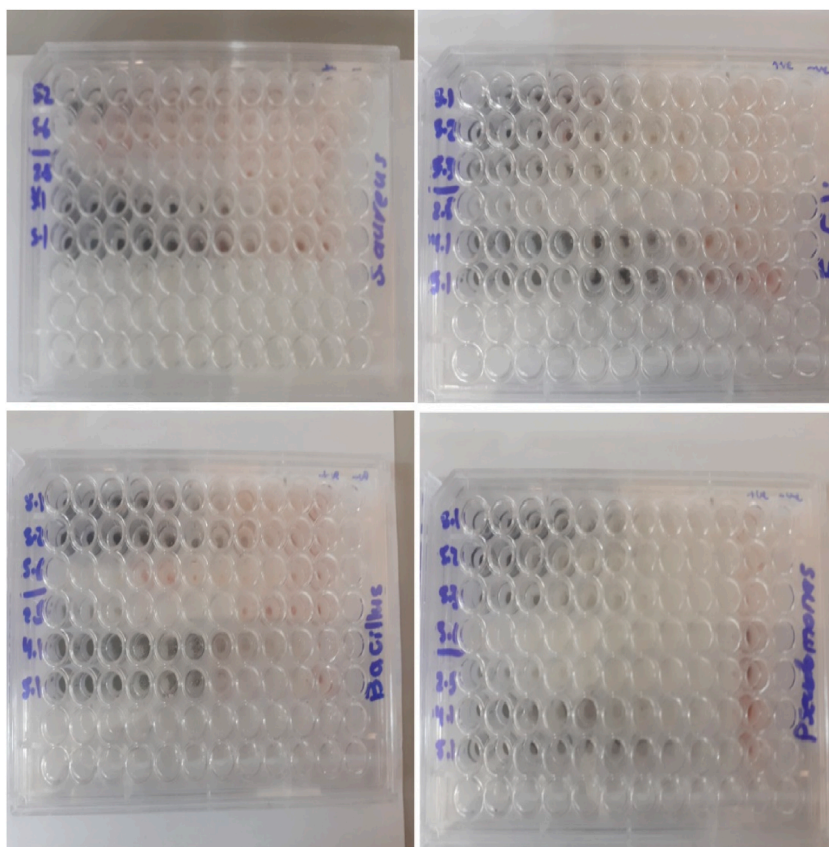
Fig. 18. MIC titer plates.

Table 6
MIC values in (mg/mL) of nanocomposites powder.

Nanocomposite	Bacterial strain							
	Gram Positive (+)				Gram Negative (−)			
	S. aureus		B. Stearothermophilus		*E. coli*		*P. aeruginosa*	
	MIC (mg/mL)	Conc. (mg/mL)	MIC (mg/mL)	Conc. (mg/mL)	MIC (mg/mL)	Conc. (mg/mL)	MIC (mg/mL)	Conc. (mg/mL)
AC	4	1.6	4	1.6	4	1.6	4	1.6
ZnO-NPs/AC	4	6.25	10	0.007	3	1	10	0.007
ZnO-NPs/AC@SiO$_2$,	2	2	7	0.062	3	1	10	0.007
ZnO-NPs/AC@SiO$_2$@mSiO$_2$	3	12.5	4	6.25	9	0.015	10	0.007
ZnO-NPs@SiO$_2$@ mSiO$_2$-Gly.	1	4	3	1	3	12.5	10	0.007
ZnO-NPs@SiO$_2$ @mSiO$_2$-*N*-halamine-Gly	4	0.0237	10	0.0003	1	0.38	4	0.0237

glycinate silane (Gly-S) agent, then chlorinated with sodium hypochlorite (Fig. 1).

XRD results revealed the presence of hexagonal structure of crystalline ZnO NPs into AC or its coated silica and mesoporous silica precursors. FTIR spectra showed interaction between the coating ZnO-NPs and AC substrate as well as its interaction with silica and mesoporous silica precursors. SEM, TEM images revealed that ZnO-NPs were well dispersed onto the mesoporous AC as well as silica and mesporous silica. There is a slight decrease in surface area of AC from 800 m^2/g due to 772 m^2/g after impregnation of AC with ZnO-PNs. The significant decrease in surface area from 772 m^2/g to 283 m^2/g and to 138 m^2/g upon silica and m-silica coating, respectively. This is probably due to silica and mesoporous silica coating of ZnO/AC. The drop of surface area to 15 m^2/g upon functionalization S-Gly is probably due to blocking of large pores and cavities of AC.

These materials have clearly showed different antimicrobial activities against all four bacterial types (two Grame positive and two Grame negative) with higher antimicrobial against the two Grame positive bacteria than the two Grame negative ones. The *N*-halamine-Gly nanocomposite reveals highest inhibition zone for all four bacterial types than that of other nanocomposite materials.
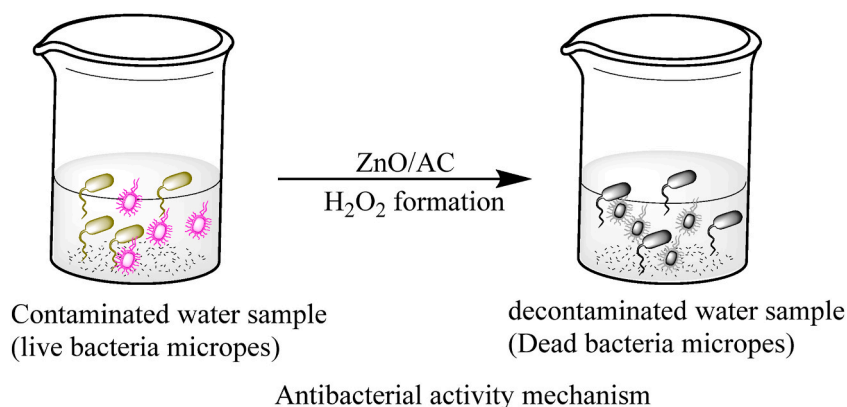
Data availability statement

Data will be made available upon request.

CRediT authorship contribution statement

Issa M. El Nahhal: Writing - original draft, Supervision, Resources, Project administration, Methodology, Formal analysis, Conceptualization. **Jamil K. Salem:** Supervision, Methodology, Investigation, Data curation. **Fawzi S. Kodeh:** Software, Methodology, Formal analysis, Data curation. **Rana H. Idais:** Visualization, Investigation, Formal analysis, Data curation, Conceptualization. **Hayfa Habes Almutairi:** Validation, Investigation, Funding acquisition, Formal analysis, Conceptualization.

Declaration of competing interest

The authors declare that they have no known competing financial interests or other personal benefits that could appeared due to this work.

Acknowledgements

References

[1] N. Bala, S. Saha, M. Chakraborty, M. Maiti, S. Das, R. Basu, P. Nandy, Green synthesis of zinc oxide nanoparticles using Hibiscus subdariffa leaf extract: effect of temperature on synthesis, anti-bacterial activity and anti-diabetic activity, RSC Adv. 5 (2015) 4993–5003, https://doi.org/10.1039/C4RA12784F.

[2] M. Om Prakash, G. Raghavendra, S. Ojha, Manoj Panchal, Characterization of porous activated carbon prepared from arhar stalks by single step chemical activation method, Mater, Today Off.: Proce. 39 (2021) 1476, https://doi.org/10.1016/j.matpr.2020.05.370, 148.

[3] K. Charoensook, C.L. Huang, H.C. Tai, V.V. Lanjapalli, L.M. Chiang, S. Hosseini, Y.T. Lin, Y.Y. Li, Preparation of porous nitrogen-doped activated carbon derived from rice straw for high-performance supercapacitor application, J. Taiwan Inst. Chem. Eng. 120 (2021) 246–256, https://doi.org/10.1016/j.jtice.2021.02.021.

[4] M.H. Kahsay, A. Tadesse, D. Ramadevi, N. Belachew, K. Basavaiah, Green synthesis of zinc oxide nanostructures and investigation of their photocatalytic and bactericidal applications, RSC Adv. 9 (2019) 36967–36981, https://doi.org/10.1039/C9RA07630A.

[5] K. Dulta, G.K. Ağceli, P. Chauhan, R. Jasrotia, P. Chauhan, A novel approach of synthesis zinc oxide nanoparticles by Bergenia ciliata rhizome extract: antibacterial and anticancer potential, J. Inorg. Organomet. Polym. Mater. 31 (2021) 180–190, https://doi.org/10.1007/s10904-020-01684-6.

[6] J. Luo, K. Fu, D. Yu, K.D. Hristovski, P. Westerhoff, J.C. Crittenden, Review of advances in engineering nanomaterial adsorbents for metal removal and recovery from water: synthesis and microstructure impacts, ACS ES&T Eng 1 (2021) 623–666, https://doi.org/10.1021/acsestengg.0c00174.

[7] M.O. Omorogie, J.O. Babalola, M.O. Ismaeel, J.D. McGettrick, T.M. Watson, D.M. Dawson, M. Carta, M.F. Kuehnel, Activated carbon from Nauclea diderrichii agricultural waste–a promising adsorbent for ibuprofen, methylene blue and CO2, Adv. Powder Technol. 32 (2021) 866–874, https://doi.org/10.1016/j.apt.2021.01.031.

[8] S. Hassan, D. Abol-Fotouh, E. Salama, MF. Elkady, Assessment of antimicrobial, cytotoxicity, and antiviral impact of a green zinc oxide/activated carbon nanocomposite, Sci. Rep. 12 (2022) 8774, https://doi.org/10.1038/s41598-022-12648-w.

[9] A.M. Aljeboree, A.B. Mahdi, Synthesis highly active surface of ZnO/AC nanocomposite for removal of pollutants from aqueous solutions: thermodynamic and kinetic study, Appl. Nanosci. 13 (2023) 943–956, https://doi.org/10.1007/s13204-021-01946-w.

[10] I.M. El Nahhal, J.K. Salem, S.K. Sylvia, T.M. Hammad, R. Hempelmann, S. Al-Bohisi, Synthesis and characterization of silica-, meso-silica- and their functionalized silica-coated copper oxide nanomaterials, J Sol-Gel Technology 79 (2016) 573–583, https://doi.org/10.1007/s10971-016-4034-z.

[11] I.M. El Nahhal, J.K. Salem, S.K. Sylvia, T.M. Hammad, R. Hempelmann, S. Al-Bohisi, Synthesis & characterization of silica coated and functionalized silica coated zinc oxide nanomaterial, Powder Technol. 287 (2016) 439–446, https://doi.org/10.1016/j.powtec.2015.09.042.

[12] B. Jurado-Sanchez, S. Sattayasamitsathit, W. Gao, L. Santos, Y. Fedorak, V.V. Singh, J. Orozco, M. Galarnyk, J. Wang, Self-propelled activated carbon Janus micromotors for efficient water purification, Small 11 (2015) 499–506, https://doi.org/10.1002/smll.201402215.

[13] W. Weber, M. Pirbazari, G. Melson, Biological growth on activated carbon: an investigation by scanning electron microscopy, Environ. Sci. Technol. 12 (1978) 817–819, https://doi.org/10.1021/es60143a005.

[14] A.K. Camper, M.W. Lechevallier, S.C. Broadaway, G.A. Mcfeters, Bacteria associated with granular activated carbon particles in drinking water, Appl. Environ. Microbiol. 52 (1986) 434–438, https://doi.org/10.1128/aem.52.3.434-438.1986.

[15] T.K.M.P. Kumar, Highly efficient performance of activated carbon impregnated with Ag, ZnO and Ag/ZnO nanoparticles as antimicrobial materials, RSC Adv. 5 (2015) 108034–108043, https://doi.org/10.1039/C5RA19945J.

[16] C. Karthik, K.V. Radha, Silver nanoparticle loaded activated carbon: an escalated nanocomposite with antimicrobial property, Orient, J. Chem. 32 (2016) 735–741, https://doi.org/10.13005/ojc/320182.

[17] Q.L. Shimabuku, F.S. Arakawa, M. Fernandes Silva, P. Ferri Coldebella, T. Ueda Nakamura, M.R. Fagundes Klen, R. Bergamasco, Water treatment with exceptional virus inactivation using activated carbon modified with silver (Ag) and copper oxide (CuO) nanoparticles, Environ. Technol. 38 (2017) 2058–2069, https://doi.org/10.1080/09593330.2016.1245361.

[18] L. Zhiyuan, Y. Shuili, P. Heedeung, Y. Qingbin, L. Guicai, L. Qi, Impact of titanium dioxide nanoparticles on the bacterial communities of biological activated carbon filter intended for drinking water treatment, Environ. Sci. Pollut. Res. 23 (2016) 15574–15583, https://doi.org/10.1007/s11356-016-6742-x.

[19] F. Wahid, Y.-X. Duan, X.-H. Hu, L.-Q. Chu, S.-R. Jia, J.-D. Cui, C.A. Zhong, Facile construction of bacterial cellulose/ZnO nanocomposite films and their photocatalytic and antibacterial properties, Int. J. Biol. Macromol. 132 (2019) 692–700.

[20] T. Huang, R. Zhou, J. Cui, J. Zhang, X. Tang, S. Chen, J. Feng, H. Liu, Fast and cost-effective preparation of antimicrobial zinc oxide embedded in activated carbon composite for water purification applications, Mater. Chem. Phys. 206 (2018) 124–129, https://doi.org/10.1016/j.matchemphys.2017.11.044.

[21] G. Qu, G. Fan, M. Zhou, X. Rong, T. Li, R. Zhang, J. Sun, D. Chen, Graphene-modified ZnO nanostructures for low-temperature NO2 sensing, ACS Omega 4 (2019) 4221–4232, https://doi.org/10.1021/acsomega.8b03624.

[22] I.M. El Nahhal, M. Al Aqad a, F.S. Kodeh, Z.S. Safi, N. Wazzan, N Halamine-modified mesoporous silica for water disinfection, Mater. Chem. Phys. 293 (2023) 126936, https://doi.org/10.1016/j.matchemphys.2022.126936.

[23] A. Taha, M. BenAissa, E. Da'na, Green synthesis of an activated carbon-supported Ag and ZnO nanocomposite for photocatalytic degradation and its antibacterial activities, Molecules 25 (2020) 1586, https://doi.org/10.3390/molecules25071586.

[24] M. Kaseem, Z. Ur Rehman, S. Hossain, A.K. Singh, B. Dikici, A review on synthesis, properties, and applications of polyactic acid silica/composite, Polymers13 303 (2021), https://doi.org/10.3390/polym13183036.

[25] S. Ntakirutimana, W. Tan, Y. Wang, Enhanced surface activity of activated carbon by surfactants synergism, RSC Adv. 9 (2019) 26519–26531, https://doi.org/10.1039/C9RA04521J.

[26] H.M. El Refay, A.M. Hyba, G.A. Gaber, Characterization and corrosion feature evaluation of mild steel in 1 M HCl by nanoparticle-modified activated carbon, Chem. Pap. 76 (2022) 813–825, https://doi.org/10.1039/C9RA04521J.

[27] I. Fatimah, S.P. Yudha, K.D. Sopiana, DL. Ratnasari, Effect of Zn Content on the Physicochemical Characteristics and Photoactivity of ZnO Supported Activated Carbon, O. J. OF CHEMISTRY, 2016, https://doi.org/10.13005/ojc/320550.

[28] J.T. Newberg, C. Goodwin, C. Arblel, Y. Khalifa, J.A. Boscoboinik, S. Rani, ZnO(101) surface hydroxylation under ambient water vapor, J. Phys. Chem. B 122 (2018) 472–478, https://doi.org/10.1021/acs.jpcb.7b03335.

[29] D. Barreca, A. Gasparotto, C. Maccato, C. Maragno, E. Tondello, ZnO nanoplatelets obtained by chemical vapor deposition studied by XPS, Surf. Sci. Spectra 14 (2007) 19–26, https://doi.org/10.1116/11.20071001.

[30] J. Das, C. Debnath, H. Nath, R. Saxena, Antibacterial effect of activated carbons prepared from some biomasses available in North East India,Energy, Sour. Part A: recover. Util, Environ. Eff. 44 (2019) 4928–4938, https://doi.org/10.1080/15567036.2019.1656305.

[31] H. Shokry, M. Elkady, E. Salama, Eco-friendly magnetic activated carbon nano-hybrid for facile oil spills separation, Sci. Rep. 10 (2020) 10265, https://doi.org/10.1038/s41598-020-67231-y.

[32] M.S. Nasrollahzadeh, M. Hadavifar, S.S. Ghasemi, M.A. Chamjangali, Synthesis of ZnO nanostructure using activated carbon for photocatalytic degradation of methyl orange from aqueous solutions, Appl. Water Sci. 8 (2018), https://doi.org/10.1007/s13201-018-0750-6.

[33] N. Ghaffar, S. Javad, M.A. Farrukh, A.A. Shah, M.K. Gatasheh, B.M.A. Al-Munqedhi, O. Chaudhry, Metal Nanoparticles Assisted Revival of Streptomycin against MDRS Staphylococcus aureus, PLOS ONE, 2022, https://doi.org/10.1371/journal.pone.0264588.

[34] Y.N. Slavin, J. Asnis, U.O. Hńfeli, H. Bach, Metal nanoparticles: understanding the mechanisms behind antibacterial activity, J. Nanobiotechnol. 15 (2017), https://doi.org/10.1186/s12951-017-0308-z.

[35] M. Balouiri, M. Sadiki, S.K. Ibnsouda, Methods for in vitro evaluating antimicrobial activity: a review, Journal of Pharmaceutical Analysis 6 (2016) 71–79, https://doi.org/10.1016/j.jpha.2015.11.005.

[36] L.B. Reller, M. Weinstein, J.H. Jorgensen, M.J. Ferraro, Antimicrobial susceptibility testing: a review of general principles and contemporary practices, Clin. Infect. Dis. 49 (2009) 1749–1755, https://doi.org/10.1086/647952.

[37] M. Bubonja-Šonje, S. Knežević, M Abram, Challenges to Antimicrobial Susceptibility Testing of Plant-Derived Polyphenolic Compounds, Arh Hig Rada Toksikol. 71, 2020, https://doi.org/10.2478/aiht-2020-71-3396.

[38] T. Ohira, O. Yamamoto, Y. Iida, Z.e. Nakagawa, Antibacterial activity of ZnO powder with crystallographic orientation, J. Mater. Sci. Mater. Med. 19 (2008) 1407–1412, https://doi.org/10.5897/AJMR10.159.

[39] J. Sawai, E. Kawada, F. Kanou, H. Igarashi, A. Hashimoto, T. Kokugan, M. Shimizu, Detection of active oxygen generated from ceramic powders having antibacterial activity, J. Chem. Eng. Jpn. 29 (1996) 627–633, https://doi.org/10.1252/jcej.29.627.

[40] X. Xu, D. Chen, Z. Yi, M. Jiang, L. Wang, Z. Zhou, X. Fan, Y. Wang, D. Hui, Antimicrobial mechanism based on H2O2 generation at oxygen vacancies in ZnO crystals, Langmuir 29 (2013) 5573–5580, https://doi.org/10.1021/la400378t.